Effects of water droplet evaporation on propagation of premixed spherical flames

Yijie Zhuang, Huangwei Zhang
Department of Mechanical Engineering, National University of Singapore
Singapore 117576, Singapore

1 Introduction

Droplet evaporation has attracted many researchers' attentions for decades, because of its importance in practical applications, like in fire suppression for civil infrastructures (e.g. buildings) and also space vehicles (e.g. manned spaceships) [1]. It is well known that water mist is an effective fire-suppression agent and has been developed for commercial practice.

Scientifically, the comprehensive interactions between continuous gas phase and dispersed liquid phase can be interpreted in terms of inter-phasic exchanges of mass, momentum, energy and chemical species [2]. There have been numerous investigations available on water-droplet-laden combustion, and most of them are concentrated on understanding weakening (or "suppression" in fire science) of the gaseous flames caused by the dispersed water droplets. It is found that water mist is more effective than inert agents (e.g. nitrogen) in reducing the burning velocity [3]. Also, addition of water droplet into the air stream can decrease the extinction strain rate in counterflow configurations [4,5]. These findings are also confirmed by the numerical simulations of freely propagating hydrogen-, methane- and propane-air flames laden with water droplets made by Kee and his co-workers [6,7]. Greenburg and Dvorjetski investigate the effects of polydispersed water spray on extinction of counterflow polydispersed spray flame and gaseous diffusion flames [8,9]. The propagating spherical gaseous flames have been extensively adopted to understand flame initiation and propagation, because of their geometrical simplicity, e.g. in Refs. [10,11]. For multi-phase spherical flames, Greenberg [12] derives an evolution equation to evaluate the finite-rate evaporation and droplet drag effects for the first time. Han and Chen [13] investigate the effects of finite-rate droplet evaporation on the ignition and propagation of premixed spherical spray flame.

The present work aims to conduct the theoretical analysis on premixed spherical flame propagation in the combustible gas mixture with water droplets. The focus is to examine the effects of initial droplet mass loading on flame propagation speed, temperature, evaporation onset and completion fronts. The mathematical model used in this work is similar to that in Refs. [14] and [15] for the laminar droplet-laden planar and spherical flames. In this work, we further extend our previous analysis in Ref. [15] for droplet-laden spherical flames, through considering the variable locations of droplet evaporation completion.

Correspondence to: mpezhuan@nus.edu.sg

2 Theoretical Analysis

We consider a 1D laminar spherical premixed flame with water droplets. Our model uses four regions (see Fig. 1) to describe fuel combustion and droplet evaporation process [12]. The four regions are respectively demarcated by the evaporation onset front (η_v), reaction front and evaporation completion front (η_{cp}). It is assumed that activation energy is infinitely large and thermal properties of gas phase (e.g. density) are constant [10,11]. Meanwhile, droplets are assumed to be monodispersed and dilute with only effect of heat exchange on reaction system [14, 15].

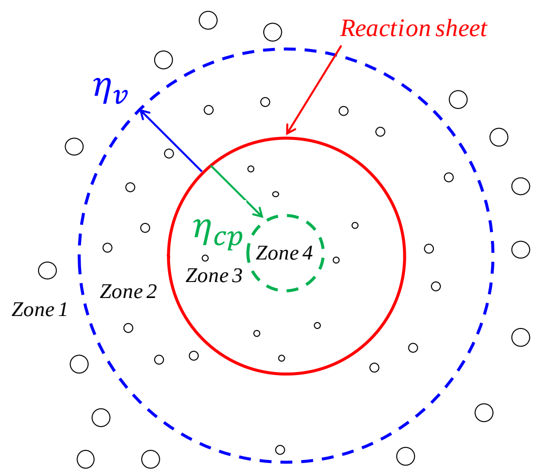

Figure 1. Schematic of a droplet-laden spherical flame. Zones 1, 2, 3, and 4 represent pre-evaporation zone, pre-flame zone, post-flame zone and post-evaporation zone, respectively.

By attaching the coordinate to the moving flame front ($\eta = r - R_f$), the dimensionless governing equations under the assumptions of quasi-steady state and large flame radius ($R_f >> 1$) are

$$-U\frac{\partial T}{\partial \eta} = \frac{1}{(\eta+R_f)^2}\frac{\partial}{\partial \eta}\left[(\eta+R_f)^2\frac{\partial T}{\partial \eta}\right] + \omega_c - \Omega(T - T_v), \tag{1}$$

$$-U\frac{\partial Y_F}{\partial \eta} = Le^{-1}\frac{1}{(\eta+R_f)^2}\frac{\partial}{\partial \eta}\left[(\eta+R_f)^2\frac{\partial Y_F}{\partial \eta}\right] - \omega_c, \tag{2}$$

$$-U\frac{\partial Y_d}{\partial \eta} = -\frac{\Omega}{q_v}(T - T_v), \tag{3}$$

where T, Y_F, Y_d are temperature, fuel and droplet mass concentrations, respectively. $U = \mathrm{d}R_f/dt$ and R_f are flame propagation speed and radius. Le is the Lewis number. Ω denotes the heat exchange coefficient due to water droplet evaporation, T_v the boiling point, ω_c the reaction rate, and q_v the latent heat of evaporation.

Equations (1-3) can be solved analytically subject to the boundary conditions and jump conditions [14, 15]. Due to the space limitation, the analytical solutions of T, Y_F, Y_d are not shown here. One can obtain the following algebraic system for the relation between U and R_f

$$\frac{2+R_fU}{R_f(\gamma_1-\gamma_2)}T_v\left(\gamma_1 e^{-\eta_v\gamma_1} - \gamma_2 e^{-\eta_v\gamma_2}\right) + \frac{T_f - T_v}{e^{-\eta_{cp}\gamma_1}/\gamma_1 - e^{-\eta_{cp}\gamma_2}/\gamma_2}\left(e^{-\eta_{cp}\gamma_1} - e^{-\eta_{cp}\gamma_2}\right) = \frac{2+LeR_fU}{LeR_f} = \left[\sigma + (1-\sigma)T_f\right]^2 exp\left[\frac{Z}{2}\frac{T_f - 1}{\sigma+(1-\sigma)T_f}\right]. \tag{4}$$

Here $\gamma_{1,2} = 0.5\left[-2/R_f - U \pm \sqrt{4\Omega + \left(2 + R_f U\right)^2 / R_f^2}\right]$, σ is the thermal expansion ratio and Z is the Zel'dovich number.

Continuity of the temperature at flame front (T_f) leads to the following implicit expression to determine the front of onset of evaporation (η_v)

$$T_f = T_v - \frac{2+R_f U}{R_f(\gamma_1-\gamma_2)} T_v\left(e^{-\eta_v \gamma_1} - e^{-\eta_v \gamma_2}\right). \tag{5}$$

The general correlation between the front of onset (η_v) and completion (η_{cp}) of evaporation is derived as

$$\delta + \frac{\Omega}{U q_v} \frac{2+R_f U}{R_f(\gamma_1-\gamma_2)} T_v\left(-\frac{e^{-\eta_v\gamma_1}-1}{\gamma_1} + \frac{e^{-\eta_v\gamma_2}-1}{\gamma_2}\right) = \frac{\Omega}{U q_v} \frac{T_f - T_v}{e^{-\eta_{cp}\gamma_1}/\gamma_1 - e^{-\eta_{cp}\gamma_2}/\gamma_2}\left(\frac{e^{-\eta_{cp}\gamma_1}-1}{\gamma_1\gamma_1} - \frac{e^{-\eta_{cp}\gamma_2}-1}{\gamma_2\gamma_2}\right). \tag{6}$$

Here δ is the water droplet mass fraction is fresh mixture. Eqs. (4-6) can be numerically solved, and the effects of initial droplet mass loading (δ), Lewis number (*Le*) and heat exchange coefficient (Ω) on spherical flame propagation can be assessed.

3 Results and Discussion

The constants used in the following analysis include [13,14,15]: the Zel'dovich number Z = 10, thermal expansion ratio σ = 0.15, boiling point T_v = 0.222, latent heat of evaporation q_v = 1.256, and evaporation induced heat exchange coefficient Ω = 0.02.

Figures 2a and 2b show the dependencies of flame propagation speed U and flame temperature T_f on flame radius R_f at various droplet mass loadings δ. Noted that the droplet evaporation onset and completion fronts are moving with the flame front during the evaporation process. As shown in Fig. 2a, the region beyond the dash-dotted line denotes the *U*-*R* solutions when droplets vaporize completely in the post-flame zone, within which there exists upper flame branches and C-shaped flame branches. When δ is relatively small (e.g. 0.1), only the upper fast flame branch can be observed. Along that, the flame propagation speed slightly increases with R_f and finally tends to be approximately 0.75 at large R_f. As δ increases to 0.2, except the upper stable strong flame branch (line a-b) with large U, a C-shaped curve with an unstable branch (dashed line c-d) and a stable weak flame branch (continuous line c-e) with small U begins to arise. Along line c-e, U decreases with R_f until reaching the boundary at $\eta_{cp} = 0$. This indicates that the droplets gradually vaporize completely in the burned zone ($\eta_{cp} < 0$), and droplets will only exist in the unburned zone ($\eta_{cp} > 0$). It is seen that line a-b is nearly unchanged with δ while the C-shaped curve becomes longer and the turning point *c* is closer to small U and R_f. In the lower stable weak flame branch, U decreases with R_f in a more sharply manner at larger δ. This is because that the strong cooling effect due to more droplet mass loading will further suppress the flame propagation speed. The high-speed and low-speed combustion modes of flame propagation are consistent with Ref. [14].

Similarly, T_f has the same bifurcation laws with increased δ. The upper stable flame branch of flame propagating speed U in Fig. 2a corresponds to the upper branch for T_f in Fig. 2b. The flame temperature in fast flame branch keeps nearly a constant value. For a fixed δ, the flame temperature decreases with R_f in the weak flame branch. It is not hard to understand that droplets with larger δ have stronger cooling effect during the evaporation process. Hence, for a fixed R_f, U and T_f decrease with δ in the weak stable flame branch. To further compare the two stable branches, two viewpoints are then set to investigate their corresponding flame structures (will be explained in Fig. 4).

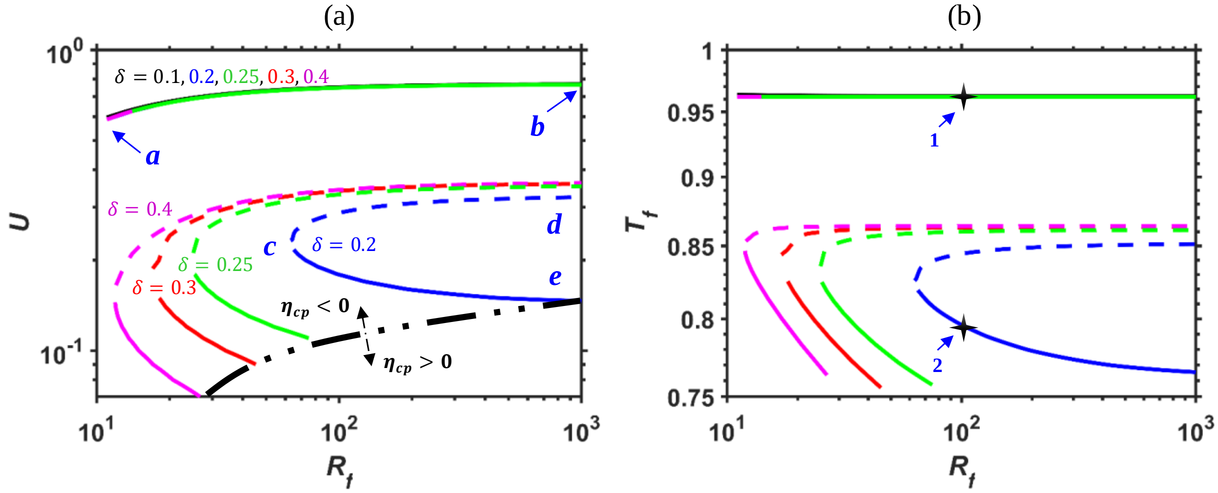

Figure 2. Flame propagation speed (a) and flame temperature (b) as functions of flame radius for different δ.

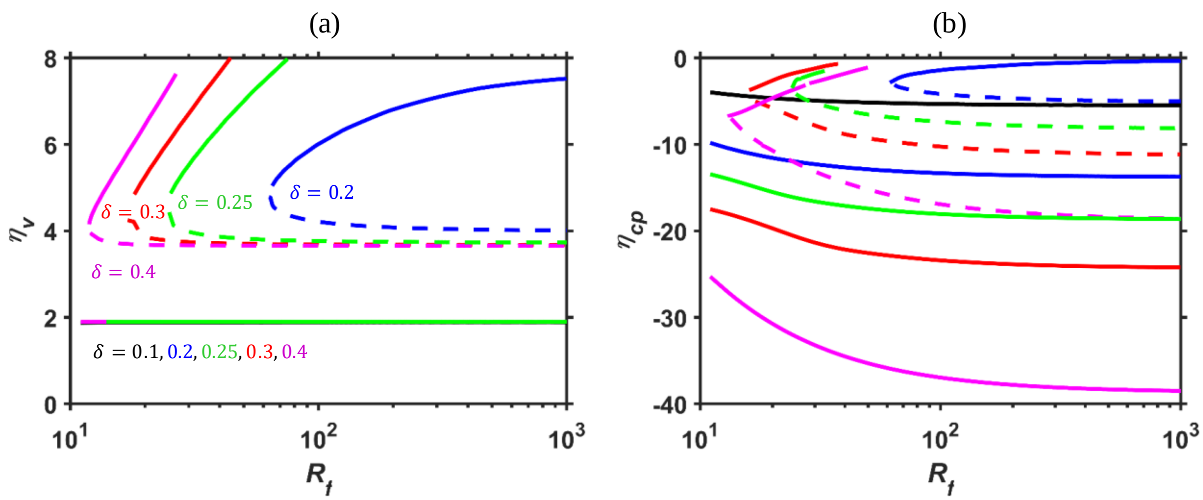

Figure 3. Front of onset (a) and complete (b) of evaporation as functions of flame radius for different δ.

The effects of mass loading δ on droplet evaporation onset front η_v and completion front η_{cp} are plotted in Figs. 3a and 3b. The upper (lower) stable flame branch of U in Fig. 2a corresponds to the lower (upper) branch for η_v and η_{cp} in Figs. 3a and 3b, respectively. As shown in Fig. 3a, the lower stable branch of η_v is nearly unchanged with δ and R_f. However, in the upper stable branch of η_v, it is directly affected by U and T_f. The more droplet mass loading, the earlier the droplets begin to vaporize, then the droplets vaporize completely quickly in the burned zone ($\eta_{cp} < 0$). Hence, as shwon in Fig. 3b, the larger the initial mass loading δ, the quicker the η_{cp} reaches 0 with smaller R_f, i.e. in the early stage of flame propagation. Here the boundary of U-R curves between $\eta_{cp} < 0$ and $\eta_{cp} > 0$ in Fig. 2a can be derived from Fig. 3b that the upper stable branch of η_{cp} increases with R_f and reaches $\eta_{cp} = 0$ at a value of R_f. Moreover, for lower stable branch of η_{cp}, it decreases with R_f and finally tends to a constant.

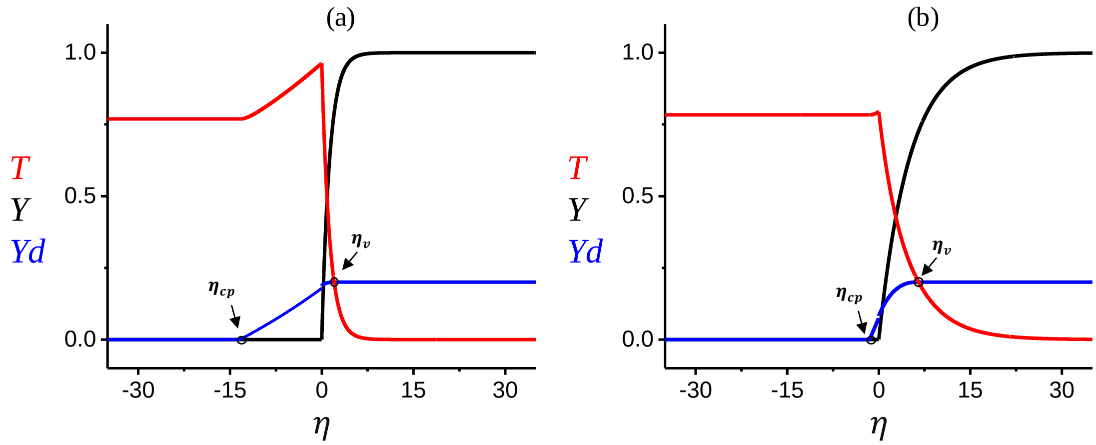

Figure 4. Flame structures for viewpoint 1 (a) and viewpoint 2 (b) shown in Fig. 2b at R_f = 100.0 and $\delta = 0.2$.

Figures 4a and 4b show the flame structures (T, Y and Y_d) for viewpoints 1 and 2 in Fig. 2b at R_f = 100 and $\delta = 0.2$. Here, viewpoints 1 and 2 represent the strong stable flame branch and weak stable flame branch, respectively. In the strong stable flame branch, the temperature of viewpoint 1 near the flame front ($\eta = 0$) reaches the boling point more quickly, hence the evaporation onset front η_v (1.895) in Fig. 4a is more closer to the flame front (0) than η_v (6.0) in Fig. 4b. Then with the same mass loading, the eavporation completion front η_{cp} (-13.34) of strong flame branch (i.e. viewpoint 1) is farther from flame front than that (-1.5) of weak flame branch (i.e. viewpoint 2).

Moreover, one can see from Fig. 4a that the temperature is highest at the flame front and then gradually decreases towards η_{cp} and keeps unchanged in the post-η_{cp} zone. This is mainly because that the water droplets vaporize in post-flame zone, which decreases the temperature of the combustion products. Also, the temperature gradient in the post-flame zone also reduces the flame temperature through heat conduction and thereby weakens the flame reactivity as well. In the pre-flame zone, the temperature in Fig. 4a decreases more sharply as compared with that in Fig. 4b.

4 Conclusions

In this study, we develop a theoretical model for flame propagation in premixed gas mixture containing water droplets, by considering droplet evaporation in the post-flame zone. Analytical correlations between flame propagating speed (U), flame front temperature (T_f), flame radius (R_f), front of onset (η_v) and completion (η_{cp}) of evaporation are derived to investigate the spherical flame propagation behavior, with emphasis on the effects of initial mass loading (δ) on spherical flames. It is found that there exists a single stable flame branch or two stable and one unstable flame branch for spherical flame, depending on initial mass loading (δ). Within the strong stable steady-state (i.e. high speed flame regime), U, T_f and η_v is almost unchanged with initial mass loading (δ), but η_{cp} decreases with δ. In the weak stable branch (i.e. low speed regime), the droplets with larger δ are more effective in reducing U and T_f but increasing η_v and η_{cp}.

Acknowledgements

YZ is financially supported by Research Scholarship Budget from National University of Singapore.

References

[1] Grant G, Brenton J, Drysdale D. (2000). Fire suppression by water sprays. Prog. Energy Combust. Sci. 26:79.

[2] Crowe CT, Schwarzkopf JD, Sommerfeld M, Tsuji Y. (2011). Multiphase Flows with Droplets and Particles, 2nd Edition. CRC Press.

[3] Fuss SP, Chen EF, Yang W, Kee JR, Williams BA, Fleming JW. (2002). Inhibition of premixed methane/air flames by water mist. Proc. Combust. Inst. 29:361.

[4] Naito H, Uendo T, Saso Y, Kotani Y, Yoshida A. (2011). Effect of fine water droplets on extinguishment of diffusion flame stabilized in the forward stagnation region of a porous cylinder. Proc. Combust. Inst. 33:2563.

[5] Yoshida A, Kashiwa K, Hashizume S, Naito H. (2015). Inhibition of counterflow methane/air diffusion flame by water mist with varying mist diameter. Fire Saf. J. 71:217.

[6] Modak AU, Abbud-Madrid A, Delplanque JP, Kee RJ. (2006). The effect of mono-dispersed water mist on the suppression of laminar premixed hydrogen-, methane-, and propane-air flames. Combust. Flame 144:103.

[7] Yang W, Kee JR. (2002). The Effect of Monodispersed Water Mists on the Structure , Burning Velocity , and Extinction Behavior of Freely. Combust. Flame 130:322.

[8] Dvorjetski A, Greenberg JB. (2002). Analysis of extinction of counterflow polydisperse spray diffusion flames by a polydisperse water spray. Proc. Combust. Inst. 29:385.

[9] Dvorjetski A, Greenberg JB. (2004). Theoretical analysis of polydisperse water spray extinction of opposed flow diffusion flames. Fire Saf. J. 39:309.

[10] He L. (2000). Critical conditions for spherical flame initiation in mixtures with high Lewis numbers. Combust. Theory Model. 4:159.

[11] Chen Z, Ju Y. (2007). Theoretical analysis of the evolution from ignition kernel to flame ball and planar flame. Combust. Theory Model. 11:427.

[12] Greenberg JB. (2007). Finite-rate evaporation and droplet drag effects in spherical flame front propagation through a liquid fuel mist. Combust. Flame 148:187.

[13] Han W, Chen Z. (2015). Effects of finite-rate droplet evaporation on the ignition and propagation of premixed spherical spray flame. Combust. Flame 162:2128.

[14] Belyakov NS, Babushok VI, Minaev SS. (2018). Influence of water mist on propagation and suppression of laminar premixed flame. Combust. Theory Model. 22:394.

[15] Zhuang YJ, Zhang HW. (2019). Effects of water droplet evaporation on initiation, propagation and extinction of premixed spherical flames. Int. J. Multiph. Flow.